Journal Pre-proofs

Reproducible generation of human midbrain organoids for *in vitro* modeling of Parkinson's disease

Sarah Louise Nickels, Jennifer Modamio, Bárbara Mendes-Pinheiro, Anna Sophia Monzel, Fay Betsou, Jens Christian Schwamborn

This is a PDF file of an article that has undergone enhancements after acceptance, such as the addition of a cover page and metadata, and formatting for readability, but it is not yet the definitive version of record. This version will undergo additional copyediting, typesetting and review before it is published in its final form, but we are providing this version to give early visibility of the article. Please note that, during the production process, errors may be discovered which could affect the content, and all legal disclaimers that apply to the journal pertain.
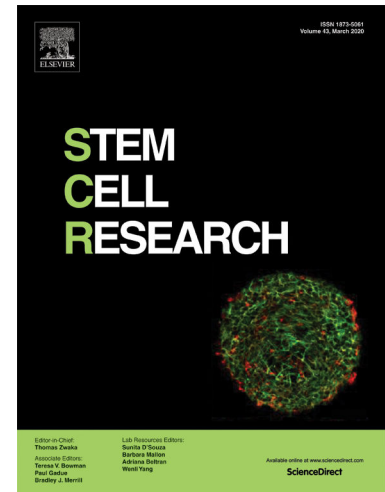
Reproducible generation of human midbrain organoids for *in vitro* modeling of Parkinson`s disease

Sarah Louise Nickels[1, 2], Jennifer Modamio[1], Bárbara Mendes-Pinheiro[1, 3, 4], Anna Sophia Monzel[1], Fay

Betsou[2] and Jens Christian Schwamborn[1,*]

[1] Luxembourg Centre for Systems Biomedicine (LCSB), University of Luxembourg, L-4367 Belvaux,
Luxembourg

[2] Integrated Biobank of Luxembourg (IBBL), Luxembourg Institute of Health, L-3555 Dudelange,
Luxembourg

[3] Life and Health Sciences Research Institute (ICVS), School of Medicine, University of Minho, Campus
de Gualtar, 4710-057 Braga, Portugal

[4] ICVS/3B's - PT Government Associate Laboratory, Braga/Guimarães, Portugal

*Corresponding author: Jens C. Schwamborn, Luxembourg Centre for Systems Biomedicine (LCSB),

University of Luxembourg, 6, avenue du Swing, L-4367 Belvaux, Luxembourg; E-mail:

jens.schwamborn@uni.lu

ABSTRACT

The study of human midbrain development and midbrain related diseases, like Parkinson`s disease (PD), is limited by deficiencies in the currently available and validated laboratory models. Three dimensional midbrain organoids represent an innovative strategy to recapitulate some aspects of the complexity and physiology of the human midbrain. Nevertheless, also these novel organoid models exhibit some inherent weaknesses, including the presence of a necrotic core and batch-to-batch variability. Here we describe an optimized approach for the standardized generation of midbrain organoids that addresses these limitations, while maintaining key features of midbrain development like dopaminergic neuron and astrocyte differentiation. Moreover, we have established a novel time-efficient, fit for purpose analysis pipeline and provided proof of concept for its usage by investigating toxin induced PD.

INTRODUCTION

Understanding the development of the midbrain dopamine system is the basis for elucidating the underlying mechanisms of diseases such as drug addiction, schizophrenia, autism, and neurodegeneration[1]. The most common age-associated midbrain disorder is Parkinson's disease (PD). PD is characterized by the irreversible loss of dopaminergic neurons in the midbrain *substantia nigra,* leading to typical motor symptoms such as bradykinesia and tremor. Despite an aging population and numerous studies in different experimental models, the progress in discovering disease-modifying treatments is slow. The lack of drugs reaching phase two clinical studies is mainly due to a deficiency in representative human models that recapitulate complex multifactorial neurological diseases [2-4]. A novel, state of the art, model system that holds great potential for studying the dopaminergic system are midbrain organoids[5-7]. These three-dimensional (3D) self-organising cellular structures mimic the

2

actual human midbrain by showing a defined spatial organization that allows differentiation into different cell types and favours their communication[8,9]. As such, compared to 2D cell culture or animal models, midbrain organoids are able to model aspects of human brain histology and physiology. Nevertheless, they still exhibit – similar to other organoid systems – certain limitations. A technical drawback is the absence of vascularization leading to an insufficient nutrient or oxygen supply in the centre of the organoid that results in a necrotic area, the so called dead core[5,7,10]. Another issue related to organoid studies is the heterogeneity in size and cellular composition. This variability affects the reproducibility of results obtained with organoids [5]. Last, the analysis techniques for 3D cell cultures are still limited, and every existing technique needs to be optimized for 3D organoids. Thus, there is a need for optimized and standardized organoid model systems. Here, we focus on midbrain organoid generation to address these limitations. We intended to generate more reproducible and viable organoids to further reduce the gap between the actual human midbrain and the currently available *in vitro* models.

RESULTS

Protocol optimization leads to smaller and earlier differentiated midbrain organoids.

In the first step of organoid standardization, we speculate that starting from a more committed cell type reduces variability between organoids. Therefore, two different guided midbrain organoid generation strategies were combined in this study[7,11]. Organoids were derived from human floor plate neuronal progenitor cells (mfNPC) similar to Smits et al.[11]. The mfNPCs were derived from three independent induced pluripotent stem cells lines (**Figure S1A** and **S1B**) and the quality of the derivation was assessed by staining with antibodies against a set of cell identity markers for stemness and midbrain (**Figure S1C**)[11,12]. Moreover, iPSC quality had been extensively assessed before for all

three cell lines in Nickels et al., 2019[38], Supplementary Figure 1. The actual midbrain organoid generation protocol was optimized based on Monzel et al. [7]. In the following, we compared three different conditions for midbrain organoid generation. Condition A represents the current standard conditions combining the two previously described protocols[7,11] (**Figure 1A**). In this condition, mfNPCs were cultivated for 8 days under maintenance conditions (Ascobic Acid (AA), LDN193189 (LDN), SB431542 (SB), Smoothened Agonist (SAG) and CHIR99021 (CHIR)) in 96 well ultralow adhesion plates in order to form 3D colonies. At day 8 they were embedded into 30 µl geltrex droplets as described by Monzel et al., favouring regionalisation[5,8]. Next at day 8, maturation was initiated in 24 well ultralow adhesion plates, under shaking conditions[7]. Maturation consists in a pre-patterning step for 3 days (Patterning I media with no LDN and SB), a patterning step for 6 days (Patterning II media reducing the concentration of CHIR) followed by a differentiation step for 21 days (AA, dbc Adenosine monophosphate (AMPc), Brain derived neurotrophic factor (BDNF), Glial derived nerurotrophic factor (GDNF), Activin A (ACT-A), Transforming growth factor beta (TGFß), (2*S*)-*N*-[(3,5-Difluorophenyl)acetyl]-L-alanyl-2-phenyl]glycine 1,1-dimethylethyl ester (DAPT)) to reach 30 days in total[11] (details described in the methods section).

In order to optimize this standard approach (Condition A), we assumed that smaller and less dense organoids, having a reduced proliferation phase, will lead to better nutrient and oxygen supply in the core and hence reduce cell death and variability. The first optimization step consisted in modifying the timing of the maturation protocol and embedding in order to reduce the maintenance phase from 8 days to 2 or 5 days respectively (Condition B and C) (**Figure 1A**). In condition B, we additionally accelerated the patterning and pre-patterning process from a total of 9 to 6 days **(Figure 1A)**. A significantly accelerated differentiation could be seen under conditions B and C, independent of the cell lines (**Figure 1B**, **1C**, **S2A-C**). This effect was more pronounced in condition B than in condition C (**Figure 1C**, **S2A** and **S2C**). Differentiation was assessed by measuring the length of the neurite outgrowth from the organoid into the surrounding matrix, the so called differentiation cloud at a specific early timepoint, here 2 days after embedding (day 10 of the process). At later stages the

4

differentiation cloud represents the neurite mass surrounding the cell bodies, however, then it is no longer representative of the neurite length, as the border of the geltrex droplet is a limiting factor forcing the neurites to bend and to intermingle.

In order to further optimize the process we investigated the effect of starting with different cell numbers for all three conditions. A total of 1000, 2000, 3000, 6000, and 9000 cells were used as starting material for colony seeding and embedding into 10 µl (1000, 2000) or 30 µl (3000, 6000, 9000) of geltrex. Colony/organoid core diameter was measured 1 day before embedding (**Figure 1D-F**, **S2D** and **S2E**) and 2 days after embedding (**Figure 1G-I** , **S2F** and **S2G**). Moreover, the size of the organoid was assed at day 30 of differentiation by measuring the Hoechst positive area representing the cell bodies, as the size of the organoid itself is limited by the geltrex droplet (**Figure 1J-L,** and **S2H-J**). Before embedding (day 7), the size of the colonies is strictly defined by the number of starting cells (**Figure 1D-F, S2G** and **S2E**)**,** however once embedded the accelerated differentiation of condition B is also significantly reducing the organoid diameter in comparison to the other conditions (**Figure 1G-I, S2F** and **S2G**). At 30 days of differentiation, when measuring the Hoechst positive area, the size of the organoid is even more dependent on the different conditions and less on the starting number of cells (**Figure 1J-L, S2H, S2J and S2K**). These observations indicate that changing the differentiation protocol is sufficient for generating smaller organoids (**Figure 1I** and **1L**). Repeating the size assessment with three different cell lines (cell line names: K7, T12 and COR), having different genetic backgrounds, ages and sex **(Figure S1B)** for the following conditions A6000, B9000, and C3000, confirmed that condition B leads to significantly smaller 1 mm (B) vs. 2 mm (A and C) organoid centre size (**Figure S2I** and **S2J**). Interestingly, this is despite the fact that condition B9000 starts with more cells at seeding than the other two conditions. A6000 (2 mm) was chosen as a control condition because it showed reduced size compared to A9000 at 30 days of differentiation (**Figure 1K**). B9000 and C3000 were chosen as further optimized conditions as they were of identical size and half the size of A6000 at 30 days (1 mm) (**Figure 1K**). Additionally, the organoid production efficiency was assessed by quantifying the

5

operators handling ability of different sized colonies during embedding. For the smallest colonies (1000 cells), half of the colonies were lost during the process (**Figure S2L** and **S2M**).

Protocol optimization reduces organoid density and enables whole mount stainings.

In a next step, the density of the dopaminergic neuron network (TH positive cells) was assessed. Therefore, the outer layer (first 205 µm) of 30 day old immunostained organoids of K7 was 3D reconstructed with the Imaris software package and the TH positive volume per organoid volume (cylinder defined by the area of the organoid and the height of the stack) was quantified (**Figure 2A-C**). The resulting density measurements showed that starting with different cell numbers (**Figure 2A-B** and **S3B**) has no impact on the dopaminergic neuron network density, whereas in condition B a significant reduction in density could be observed (**Figure 2A** and **2C** and **1J** and **S3A-B**). This decrease is inversely correlated to the antibody penetration into the organoid inner layers (**Figure 2D-F** and **S3C**). Reduced density enables increased antibody penetration. Images were taken in free floating organoids using the 5x objective and vertical planes are shown (**Figure 2D** and **S4A**). The antibody penetration up to 800 µm in condition B (**Figure 2D and 2F**) is significantly increased compared to condition A and C where only around 200 µm depth was reached (**Figure 2D** and **2F**). The reduced density (**Figure 2G**) can be explained by an equal volume of TH (**Figure 2H**) but a smaller organoid centre (**Figure 2I**). Antibody penetration in condition B for up to 800 µm is far enough to enable whole mount stainings (**Figure 2D** and **3A** and **S4A-C**). As whole mount stains drastically improve productivity and reduce labour intensity compared to staining and imaging of individual sections, we optimized this step further (**Figure 3**). Using the optimized protocol, we were able to perform whole mount stains in all of the three conditions A6000, B9000 and C3000 at day 30 of differentiation for all three cell lines (Representative images are shown) (**Figure 3**). Moreover, mounting the organoids allowed us to take 20x images throughout the whole organoid (28 stacks a 10µm) (**Figure 3** and **S4B**). Last, the whole

6

mount stainings enabled, 3D reconstruction in Imaris of the whole organoid using either the 5x (**Figure S4A**) or 20x objective (**Figure S4C**).

Optimized midbrain organoids have increased viability and no dead core.

One of the most severe limitations of many organoid systems is the presence of dead cells in the centre, reaching a size of up to 4 mm² (the so-called dead core). We next aimed at analysing the dependency of the dead core size on the starting cell number and differentiation conditions. Accordingly, we measured the size of the necrotic area in the centre of the organoid at 30 days of differentiation. Due to instability of this necrotic area, it typically falls out of organoid sections and hence appears as an empty centre in the images of the sectioned organoids (**Figure 4A**). Sections of organoids generation in condition A showed a significant dead core, which was slightly smaller when a lower number of starting cells was used (e.g. A9000 vs A3000) (**Figure 4B**). However, noticeable differences were observed when comparing conditions B and C to A. Strikingly, organoids generated according to condition B showed no dead core. While those generated according to condition C showed a small dead core in organoids starting with more than 3000 cells (**Figure 4A, 4B** and **3**). This observation is in agreement with the antibody penetration distance - and though probably nutrient supply - highlighted above (**Figure 2D-F**). Based on these results, we decided to use for the further validation, for both conditions B and C, the biggest organoids with no dead core, these correspond to condition B with a starting cell amount of 9000 cells (B9000) and condition C with a starting cell amount of 3000 cells (C3000). Importantly, B9000 and C3000 show a reduced size compared to A6000, which we chose as control condition in the further analysis (**Figure 1K**).

In order to investigate how reproducible these results are in different cell lines, the dead core measurements were repeated (**Figure 4C-E**), the pyknotic nuclei were counted (**Figure 4F-G**), live cells were counted (**Figure 4H**) and an ATP viability assay was performed (**Figure 4I** and **4J**) using three independent cell lines and the above-determined conditions. Condition B significantly reduced the

7

dead core formation to nonexistence (**Figure 4C and 4E**), the amount of pyknotic cells (measured in whole mount stainings) from 45 % to 30 % (± 2.1% standard error of difference between means) (**Figure 4F**) and more than doubled the number of live cells as well as organoid viability (**Figure 4H-I**). No significant difference between the cell lines were observable, which indicates a high degree of reproducibility for this approach (**Figure 4D**, **4G**, and **4J**).

Midbrain organoids reveal a distinct spatial regionalisation and the presence of glial cells.

After determining condition B as most favourable according to the so far analysed criteria, we investigated if the midbrain organoids derived under this condition are able to generate different cellular identities and a spatial organization (**Figure 5**). Therefore, we performed stainings for stem cell-, neuronal -and glial markers at day 30 of differentiation (**Figure 5A-O**). Both, whole mount stainings using the optimized immunohistochemistry protocol, followed by Zeiss confocal image quantification, as well as section stainings using high content automated microscopy were performed (**Figure 5A** and **5B**). Whole mout stainings show slightly squeezed organoids from the top, including all cross sections **(Figure 5C)**. Sections show the radial and tangential sections of the organoid, which is disc shaped **(Figure 5C)**. For whole mount stainings the volume of the regions stained with different markers, Hoechst, TH, TUJ1 and FOXA2 was quantified by 3D reconstruction in the Imaris software (**Figure 5A**). For sections, the mask of the markers TUJ1, GFAP, S100ß, SOX2, Hoechst, and Ki67 was generated by an in house implemented Matlab script (**Figure 5B**). Neuronal quantification in whole mount stainings by TUJ1 showed a significant increase in the amount of neurons in condition B when normalized to the volume of nuclei, independent of cell lines (**Figure 4D** and **4E**). This increase was also observed for the dopaminergic neuron marker TH (**Figure 4F and S5B**). The increase can be explained by an equal volume of TH (**Figure 2G** and **2H**) but a smaller organoid centre and lower number of cells B= 11291 ± 866 vs. A= 46061 ± 1488 (**Figure 1L, 2I and S5A**) as well as fewer dead cells (pyknotic nuclei) (**Figure 3F and 2G**). The relative percentage of TUJ1 positive cells, quantified within

sections, was 85.57 % (± 3.7 SEM) for condition B (**Figure 4G I**). In an attempt to quantify the exact amount of neurons within the organoid under the different conditions the percentage of TUJ1 positive nuclei (**Figure 4G I**) was applied on the count of alive nuclei (described in **Figure 4H**), showing that around 21071 nuclei are TUJ1 positive in condition B (**Figure 4G II**). Interestingly, the vast majority of the TUJ1 positive cells expressed TH (**Figure S5C**). Moreover, the quantification of TUJ1 over Hoechst, using the whole mount staining approach reflects the observations made in sections, validating this novel method (**Figure 5D and S5E**). Glial cell analysis in sections demonstrated that the total amount of S100ß and GFAP positive cells was 10.51 % (± 2.4 SEM) and 7.13 % (± 1.2 SEM) respectively, for condition B, which is higher than for the other conditions (**Figure 5H and 5I**). In addition, neural stem cells and progenitor cells were quantified using the stem cell marker SOX2, the proliferation marker Ki67 and the midbrain marker FOXA2 (**Figure 5J-L**). The midbrain specific neuronal progenitor and young neuron marker FOXA2 was present in 54.01 % (± 13.4 SEM) of all the cell nuclei in all the conditions (**Figure 5J**). 32.28% (± 0.06 SEM) of the cells expressed the stem cell marker SOX2 and 14.02% (± 0.04 SEM) were proliferative (**Figure 5K** and **5L**). Representative immunofluorescent stainings of the different markers are shown in **Figure 5M-O**. The three cell lines showed no significant differences for all investigated markers. Example plots are shown for TUJ1, TH, GFAP, S100β and FOXA2 for both whole mount and section quantifications (**Figure 5E, S5B, S5D and S5F-H**). Lastly, all three conditions showed inner-outer layer organization reminiscent of brain development and regionalisation with a stem cell niche resembling ventricular cavities. Typically, neural epithelial stem cells (NE) form rosette like structures and give rise to basal progenitor stem cell within the subventricular zone, here all positive for FOXa2. These progenitors then differentiate in a first wave to form a neuronal layer, followed by a second wave of astrocyte differentiation[18] (**Figure S5I**).

The optimized protocol reduces batch to batch and cell line variability.

Next, we addressed variations stemming from batch to batch differences or cell line variability **(Figure 5P and 5Q)**. Therefore, the coefficient of variation (CV) for 9 different conducted experiments was calculated. As parameters for this we chose three measurements for size (the diameter before and after embedding as well as the area of Hoechst at 30 days **(Figure 1)**); three measurements for differentiation (size of the differentiation cloud **(Figure 1)**, the volume TUJ1/Hoechst and the volume S100ß/Hoechst from the sections **(Figure 5)**) as well as three measurements related to cell death (the ATP variability assay, the size of the dead core and amount of pyknotic nuclei **(Figure 3)**). Using these 9 experimental data sets the CV was calculated for each of the 27 data points (3 cell lines, 9 experiments) across all three batches. The same was done for the CV across cell lines (27 data points from 3 batches and 9 experiments). The average CV for condition B in comparison to the control condition A, shows that the optimized protocol is significantly reducing the variability between batches from 46.62 % to 25.77 % (±8.8 standart error of differences between the means) and of differences and between cell lines from 40.33 % to 27.83 % (±5.9 standart error of differences between the means) (**Figure 5P** and **5Q**). Condition C on the other hand is not reducing the variability significantly (**Figure 5J** and **S5K**).

Optimized midbrain organoids harbour different neuronal subtypes.

In order to further reveal cellular type identities in the midbrain organoids, we assessed the presence of neuronal subtypes by immunocytochemistry at day 30 (**Figure 6**). Besides dopaminergic signalling, abundantly characterized hereafter, glutamatergic and serotonergic signalling play an import roles within the midbrain. A subset of dopaminergic neurons for instance express vesicular glutamate transporter 2 (GLUT), which when abolished leads to neurodegeneration[14]. Moreover, serotonin-expressing neurons (SERO), are thought to have besides their physiological roles, important functions in midbrain related diseases such as Parkinson's disease[15]. Here, we were able to detect both GLUT positive and SERO positive neurons that either co-expressed TH or not (**Figure 6A and 6B**). The

midbrain substantia nigra is further subdivided in different regions, and mainly dopaminergic neurons of the region A9 are affected in PD. These neurons are positive for the G protein-coupled inwardly-rectifying potassium channel 2 (GIRK2). Indeed, the here described optimized midbrain organoids consist of TH/GIRK2 double positive cells, indicating A9 dopaminergic neuron identity (**Figure 6C**). Moreover, we detected dopamine transporter (DAT) and dopamine (DOPA) itself, both bearing witness of dopamine synthesis and transport (**Figure 6D** and **6E**), as shown in more details by Smits et al. 2019[11]**.** Lastly, we could show that pre- and post-synaptic proteins such as synaptophysin (SYP) and post-synaptic density protein 95 (PSD95) are expressed, which are necessary for synaptic transmission (**Figure 6F**).

Optimized midbrain organoids are suitable to investigating toxin induced PD.

In order to validate the fitness for purpose of the optimized human midbrain organoids for neurotoxicology studies and *in vitro* modeling of PD, we used the 6-OHDa model, which is well established in rodents[16,17]. Midbrain organoids of all three iPSC cell lines produced according to condition B were treated with 50 µM, 100 µM, 150 µM and 175 µM of 6-OHDA (**Figure 7**). Treatments were performed at day 30 of differentiation for 2 consecutive days and analysis was done after 6 additional days. The number of GFAP positive cells remained unaffected by the treatment (**Figure 7A and 7B**). The volume of TH positive dopaminergic neurons, however, decreased in a dose dependent manner (**Figure 7C and S5I**). The specificity of the loss of dopaminergic neurons was assessed by quantifying the number of TUJ1 positive cells, which slightly but insignificantly decreased (**Figure 7D).** Moreover, when normalizing TH to TUJ1 the decrease upon 6OH-Da treatment remains significant (**Figure 7E**), which validates the fitness for purpose of this optimized midbrain organoid system as potential model for PD.

DISCUSSION

By modulating the organoid maturation process, we have generated a novel optimized and standardized human midbrain-like organoid model that exhibits many features reminiscent of the human midbrain dopaminergic system. The optimized generation strategy led to a spatially organized organoid model, including different cell types of neuroectodermal origin. The different cell types encompassed stem cells, neurons and glial cells and emerged in a sequence reminiscent of neuronal development, forming defined structural layers and ventricular-like structures[18]. On one hand, the optimized organoid model has a relative amount of TH-expressing dopaminergic neurons, which is not achieved in any other model [7,11]. On the other hand, the occurrence of different neuronal subtypes underlines the cellular complexity of the neuronal network. Importantly, both characteristics are necessary to model the heterogeneity of midbrain development and pathology. As an example, in PD, selectively A9 dopaminergic neurons expressing vGLUT2 have an increased vulnerability [19,20].

In this study, we successfully addressed several of the main drawbacks related to organoid production, usage, and analysis, including issues with organoid variability in properties of interest such as between lines as well as between batches, amenability to whole mount imaging, and massive cell death in the organoid centre[21]. Previous studies showed that healthy neurons are limited to the outer perimeter of the organoid because of the necrotic core[22,23]. Using a further committed cell type as starting population and an accelerated differentiation protocol, we were able to eliminate the dead core completely and to reduce cell death by 15 % in the remaining tissue. Moreover, upon the size and density reduction, a viable, FOXA2+ inner cell mass could be observed and ATP production was increased by 40% compared to control condition. In contrast to the most recent strategies that have attempted to reduce the necrotic core and enhance diffusion by specific bioreactors and the reduction of the starting cell numbers, we could show that the modulation of the organoid maturation process itself represents the critical factor [10,24,25]. Reducing tissue density seemingly resulted in a better oxygen

12

and nutrient supply[26]. The optimized neuronal induction is the key towards reduced cell death[24] and represents a big step in the usage of organoids for therapeutic approaches.

In addition, the described approach enabled whole mount stainings that permit 3D reconstruction and quantificative analysis of the whole organoid. This concept represents an efficient method to overcome the challenging and labour-intensive step of sectioning, and the mounting strategy enabled the necessary depth of stain penetration when using confocal microscopy[21]. Moreover, this approach offers a holistic perspective on the spatial distribution, localization, and relative amounts of different cell types. The more guided maturation process did not interfere with regionalization and cellular diversity. Further, compared to previous 3D reconstructions using the clarity approach, we were able to reconstruct and quantify the detailed architecture of the 3D neuronal network, enabling future automated phenotyping strategies[9]. This optimization is a breakthrough in cost and time efficient organoid analysis.

Lastly, the accelerated and more unidirectional maturation process, helped to overcome the variability resulting from spontaneous cellular commitment[27]. Using a more defined patterning strategy in order to optimize reproducibility has been previously observed in dorsally patterned forebrain organoids derived from iPSCs[28,29]. These authors have also shown that exogenous patterning, using a guided strategy, has no effect on terminal cell identities[28,30]. By starting from a more committed cell type and adapting a defined patterning strategy, we were able to reduce the variability between cell lines and between different organoid batches by half in the here described approach. Significantly, the optimization of the timing during the maturation process was revealed to be a critical factor for increased reproducibility and to overcome the batch to batch variability, also called batch syndrome[31]. The increased reproducibility, independent of the batch of the starting material, genetic background, and sex of the original donor, confirms the robustness of the method, which is a crucial characteristic for its use in clinical applications and commercialisation. Nevertheless, it should be noted that although the variability has been reduced there remain some differences.

These variations, were expected as we speak of a living biological system and should be accounted for. In order to draw valid conclusions results should ideally be observed in independent batches and cell lines.

Taken together, we demonstrate that we can generate standardized midbrain organoids in a reproducible manner, while maintaining cellular complexity of the model. The optimization strategy could potentially be extended to other organoid models facing similar limitations. As proof of concept, we validated and demonstrated the fitness for purpose of this novel organoid system, by recapitulating toxin induced dopaminergic neuronal cell death in the midbrain, modeling a form of PD[32]. This achievement, does not only demonstrates the models usefulness for analysing real-life problems, as toxin induced PD represents in some areas of the world the major cause for PD[36,37], but can also replace the well-established, highly-used and ethically-compromised 6OH-Da rodent models[16,17]. As such, the model has great potential for drug screening and will complement other model systems, as well as clinical studies designed to mechanistically investigate neurodegeneration or other midbrain diseases, in order to discover novel therapeutic approaches.

Online METHODS

mfNPC cultivation and derivation from iPSCs

mfNPCs were maintained for up to 15 passages (after their generation from iPSCs) under maintenance medium, splitted at a confluency of 80% using Accutase and seeded 600.000 cells per well on a geltrex coated 6 well plate. N2B27 maintenance media consists of equal parts DMEM HAM's F12 and Neurobasal with GlutaMAax (1:500), Pen-Strep (1:500) N2 (1:200) and B27 (–Vitamin A) (1:100). N2B27 is freshly supplemented with Ascorbic Acid 200 µM (Sigma), CHIR 99021 3 µM (Axon Medchem), SAG 0.5 µM (Merck), SB-431542 10 µM (Ascent Scientific) and LDN-193189 250 nM

(Sigma). Derivation of mfNPCs from iPSCs is described in detail in the study of Smits et al.[11] iPSCs were generated as described in the study of Reinhardt et al., or bought from Coriel.[33] K7 is derived from fibroblasts from a 81 year old female, T12 from a 53 year old female and COR from a 55 year old male. All work with human stem cells was done after approval of the national ethics board, Comité National d'Ethique de Recherche (CNER), under the approval numbers 201305/04 and 201901/01.

Organoid generation

Human mfNPCs were seeded at different densities (1000, 2000, 3000, 6000, 9000) into 96 well ultralow adhesion plates and cultivated for 30 days under different medium compositions as shown in Figure 1A for condition A, B and C. For colony formation they were kept in maintenance medium for 8d for condition A, for 2 days for condition B and 5 days for condition C. Patterning I medium consists in maintenance medium without SB and LDN and was added for condition A and C for 3 days and for condition B for 2days. For patterning II medium the concentration of CHIR was additionally reduced to 0.7 µM. Cells were kept for 6 days for condition A and C, and 4 days for condition B, in patterning II media. Differentiation medium consist in N2B27 medium with 10 ng/ml BDNF (Peprotech), 10 ng/ml GDNF (Peprotech), 200 µM AA, 500 µM dibutyryl cAMP (Sigma), 1 ng/ml TGF-β3 (Peprotech), 2.5 ng/ml ActivinA (Peprotech) and 10 µM DAPT (Cayman). Differentiation medium was added for condition A and C for 21 days, and for condition B for 24 days. At day 8, independent of the patterning strategy, the colonies were embedded into geltrex droplets as described by Monzel et al, and cultivated under shaking conditions in a 24 well ultralow adhesion plates.[7]

Immunocytochemistry

Immunofluorsecent stainings using mfNPCs were performed as described in Smits et al., Antibodies are found in Supplementary Table 1.

For staining of sections midbrain organoids were fixed at day 30 of differentiation with 4% PFA overnight at 4 °C, washed three times with PBS for 15 min and embedded in 3% low-melting point agarose. The solid agarose block was sectioned with a vibratome (Leica VT1000s) into 80 μm sections. The sections were blocked on a shaker with 0.5% Triton X-100, 2% BSA, and 5% goat or donkey serum in PBS for 90 min at RT. Primary antibodies were diluted in the same solution with 0.1% Triton X-100 and were applied for 72h at 4 °C. After incubation with the primary antibodies (see Supplementary Table 1), sections were washed three times with PBS for 10min at RT on a shaker. Then, the sections were incubated with the secondary antibodies for 2 h at RT (same solution as primary) and washed three times with PBS and once with Milli-Q water before they were mounted in Fluoromount-G mounting medium (Southern Biotech).

Whole mount stainings were performed according to a modified protocol described by Koehler et al.[34] Organoids were fixed at day 30 of differentiation with 4% PFA overnight at 4 °C, washed three times with PBS for 5 min. They were incubated for 8min in ice cold Acetone, to optimize antibody penetration (previously described for whole mount immunohistochemistry in Zebrafish eggs by Abcam). Blocking was done with 0.1% Triton X-100, 10% goat or donkey serum in PBS o/n at RT. Primary antibodies were diluted in 0.1% Triton X-100, 3% goat or donkey serum in PBS and incubated 3 days at 4 °C on a shaker. Organoids were then washed three times with PBS for 60 min at RT and secondary Antibodies were added (same solution as primary) for 2 days at 4 °C on a shaker. Finally, three washes for 5min at RT were performed using 0.05% Tween-20 in PBS and one with water. Then the organoids were mounted in Fluoromount-G mounting medium.

STAINperfect Immunostaining Kit (ImmuSmol) was used according to the manufacturer's protocol to detect dopamine in whole mount stains.

Imaging Analysis and quantification

Confocal images of entire whole-mount organoid stainings were taken using the 5x or 20x objective of the Zeiss PALM/Axiovert fluorescence microscope. Imaris 3D reconstruction software was used in order to quantify the volume of the marker (TH, TUJ1, Hoechst) expression, using the surface function. Thresholds were set manually according to visual alignment. FOXA2 and nuclei's were counted with the spot function (threshold for size per count set to 10 µm for detecting viable cells only). Pyknotic nuclei were analysed using their smaller size as discriminating factor (7 µm - 10 µm = pyknotic nucleis only) compared to the total amount of cells (threshold at 7 µm for viable and non-viable) within the spot functions.

For qualitative and representative images the 60x objective was used.

The organoid sections of 80 µm thickness were acquired with an Operetta High-Content Imaging System (Perkin-Elmer) and analysed with the following image analysis algorithm. Immunofluorescence 3D images of midbrain organoids were analysed in Matlab (Version 2017b, Mathworks). The in-house developed image analysis algorithm for automated marker quantification based on voxels was described before [11,35] and the script can be found in the online repository https://github.com/LCSB-DVB/Nickels_2019.

Brightfield images were taken using the Stereomicroscope Nikon SMZ25 or the AxioVert.A1 from Zeiss.

ATP assay

The ATP essay was perfomed using the CellTiter-Glo 3D cell viability assay (Promega) according to the manufactors protocol. Luminescence was measured using the Microplate Cytation5M Cell imaging Multi Mode Reader (Biotek). ATP luminescent levels were normalized to the organoid diameter.

Size measurements

Size was determined using the bright field or fluorescent images and by measuring the diameter or area with the Zeiss software.

Variability

The coefficient of variation was calculated for 9 experimental data sets. Three quality attributes for size: the diameter before and after embedding as well as the area of Hoechst staining at 30 days. Three quality attributes for of differentiation: the size of the differentiation cloud, the volume ratio TUJ1/Hoechst and the volume ratio S100ß/Hoechst. Three quality assessments related to cell death: the ATP production, the dead core size and the pyknotic nuclei count. For each of the quality attributes the CV was calculated across batches and across cell lines. For batch to batch variability, 27 CV's were calculated based on the variation between the three batches (9 quality attributes (experimental data sets) and 3 cell lines). For cell line variability the same was done for all three cell lines (27 data points from three batches and 9 quality attributes). The average CV of all 27 data points is shown for each condition (A, B and C). The script for calculations can be found here: https://github.com/LCSB-DVB/Nickels_2019.

6-OHDa and rotenone treatment

The 6-OHDa treatment was performed at day 30 of differentiation at two consecutive days for 24h. 6-OHDa was dissolved at concentration 50 µM, 100 µM, 150 µM and 175 µM in N2 media without growth factors (500 µl/organoid) kept on ice in the dark. The organoids then rested for additional 6 days in differentiation media before analysis.

Data availability

All data can be found under https://doi.org/10.17881/lcsb.20191008.01

AUTHOR CONTRIBUTIONS

S.N. designed and conducted the experiments, interpreted the data and drafted the manuscript. J.M. and B.P. conducted specific experiments and A.M. contributed to the manuscript. F.B. and J.C.S. coordinated and conceptualized the study. All authors reviewed and approved the final manuscript.

COMPETING INTEREST

JCS is co-founder and shareholder of the biotech company OrganoTherapeutics SARL.

REFERENCES

1. Bissonette, G.B. & Roesch, M.R. Development and function of the midbrain dopamine system: what we know and what we need to. *Genes, Brain and Behavior* **15**, 62-73 (2016).
2. Burns, T.C., Li, M.D., Mehta, S., Awad, A.J. & Morgan, A.A. Mouse models rarely mimic the transcriptome of human neurodegenerative diseases: A systematic bioinformatics-based critique of preclinical models. *European journal of pharmacology* **759**, 101-117 (2015).
3. Van der Worp, H.B.*, et al.* Can animal models of disease reliably inform human studies? *PLoS med* **7**, e1000245 (2010).
4. Hodge, R.D.*, et al.* Conserved cell types with divergent features in human versus mouse cortex. *Nature* (2019).
5. Lancaster, M.A.*, et al.* Cerebral organoids model human brain development and microcephaly. *Nature* **501**, 373-379 (2013).
6. Jo, J.*, et al.* Midbrain-like Organoids from Human Pluripotent Stem Cells Contain Functional Dopaminergic and Neuromelanin-Producing Neurons. *Cell stem cell* **19**, 248-257 (2016).
7. Monzel, A.S.*, et al.* Derivation of Human Midbrain-Specific Organoids from Neuroepithelial Stem Cells. *Stem cell reports* **8**, 1144-1154 (2017).
8. Qian, X.*, et al.* Brain-Region-Specific Organoids Using Mini-bioreactors for Modeling ZIKV Exposure. *Cell* **165**, 1238-1254 (2016).
9. Renner, M.*, et al.* Self-organized developmental patterning and differentiation in cerebral organoids. *The EMBO journal* **36**, 1316-1329 (2017).
10. Berger, E.*, et al.* Millifluidic culture improves human midbrain organoid vitality and differentiation. *Lab on a chip* (2018).
11. Smits, L.M.*, et al.* Modeling Parkinson's disease in midbrain-like organoids. *NPJ Parkinsons Dis* **5**, 5 (2019).
12. Takahashi, K. & Yamanaka, S. Induction of pluripotent stem cells from mouse embryonic and adult fibroblast cultures by defined factors. *Cell* **126**, 663-676 (2006).
13. Koehler, K.R., Mikosz, A.M., Molosh, A.I., Patel, D. & Hashino, E. Generation of inner ear sensory epithelia from pluripotent stem cells in 3D culture. *Nature* **500**, 217 (2013).
14. Shen, H.*, et al.* Genetic deletion of vesicular glutamate transporter in dopamine neurons increases vulnerability to MPTP-induced neurotoxicity in mice. *Proceedings of the National Academy of Sciences of the United States of America* **115**, E11532-E11541 (2018).
15. Grosch, J., Winkler, J. & Kohl, Z. Early Degeneration of Both Dopaminergic and Serotonergic Axons - A Common Mechanism in Parkinson's Disease. *Frontiers in cellular neuroscience* **10**, 293-293 (2016).
16. Carvalho, M.M.*, et al.* Behavioral characterization of the 6-hydroxidopamine model of Parkinson's disease and pharmacological rescuing of non-motor deficits. *Molecular neurodegeneration* **8**, 14-14 (2013).
17. Ungerstedt, U. & Arbuthnott, G.W. Quantitative recording of rotational behavior in rats after 6-hydroxy-dopamine lesions of the nigrostriatal dopamine system. *Brain research* **24**, 485-493 (1970).
18. Kriegstein, A. & Alvarez-Buylla, A. The glial nature of embryonic and adult neural stem cells. *Annual Review of Neuroscience* **32**, 149-184 (2009).
19. Hirsch, E., Graybiel, A.M. & Agid, Y.A. Melanized dopaminergic neurons are differentially susceptible to degeneration in Parkinson's disease. *Nature* **334**, 345-348 (1988).

20. Steinkellner, T*., et al.* Role for VGLUT2 in selective vulnerability of midbrain dopamine neurons. *The Journal of clinical investigation* **128**, 774-788 (2018).

21. Poli, D., Magliaro, C. & Ahluwalia, A. Experimental and Computational Methods for the Study of Cerebral Organoids: A Review. *Frontiers in neuroscience* **13**, 162-162 (2019).

22. Watanabe, M*., et al.* Self-Organized Cerebral Organoids with Human-Specific Features Predict Effective Drugs to Combat Zika Virus Infection. *Cell reports* **21**, 517-532 (2017).

23. Luo, C*., et al.* Cerebral Organoids Recapitulate Epigenomic Signatures of the Human Fetal Brain. *Cell reports* **17**, 3369-3384 (2016).

24. Quadrato, G*., et al.* Cell diversity and network dynamics in photosensitive human brain organoids. *Nature* **545**, 48-53 (2017).

25. Qian, X*., et al.* Generation of human brain region-specific organoids using a miniaturized spinning bioreactor. *Nature protocols* **13**, 565-580 (2018).

26. Ardakani, A.G., Cheema, U., Brown, R.A. & Shipley, R.J. Quantifying the correlation between spatially defined oxygen gradients and cell fate in an engineered three-dimensional culture model. *Journal of the Royal Society, Interface* **11**, 20140501-20140501 (2014).

27. Quadrato, G. & Arlotta, P. Present and future of modeling human brain development in 3D organoids. *Current opinion in cell biology* **49**, 47-52 (2017).

28. Arlotta, P. Organoids required! A new path to understanding human brain development and disease. *Nature methods* **15**, 27-29 (2018).

29. Kadoshima, T*., et al.* Self-organization of axial polarity, inside-out layer pattern , and species-specific progenitor dynamics in human ES cell-derived neocortex. *Proceedings of the National Academy of Sciences* **110**, 20284-20289 (2013).

30. Qian, X., Song, H. & Ming, G.-l. Brain organoids: advances, applications and challenges. *Development* **146**, dev166074 (2019).

31. Kelava, I. & Lancaster, M.A. Dishing out mini-brains : Current progress and future prospects in brain organoid research. *Developmental biology* **420**, 199-209 (2016).

32. Monzel, A.S*., et al.* Machine learning-assisted neurotoxicity prediction in human midbrain organoids. *bioRxiv*, 774240 (2019).

33. Reinhardt, P*., et al.* Derivation and expansion using only small molecules of human neural progenitors for neurodegenerative disease modeling. *PloS one* **8**, e59252 (2013).

34. Koehler, K.R. & Hashino, E. 3D mouse embryonic stem cell culture for generating inner ear organoids. *Nature protocols* **9**, 1229-1244 (2014).

35. Bolognin, S*., et al.* 3D Cultures of Parkinson's Disease-Specific Dopaminergic Neurons for High Content Phenotyping and Drug Testing. *Adv Sci (Weinh)* **6**, 1800927 (2019).

36. Liou H. H. *et al.*, Environmental risk factors and Parkinson's disease. *Neurology* **48**, 1583-1588 (1997).

37. Caroline M.Tanner. The role of environmental toxins in the etiology of Parkinson's disease. *Trends in Neurosciences* **12**, 49- 54 (2003).

38. Nickels L. S. *et al.* Impaired serine metabolism complements LRRK2-G2019S pathogenicity in PD patients. *Parkinsonism and related disorders* **67**, 48-55. (2019)

FIGURE LEGENDS

Figure 1. Lower number of starting cells and a different timing of the patterning reduces organoid size.

(**A**) Organoid maturation protocol. Patterning strategies A, B and Patterning I by CHIR, SAG, AA, patterning II by less CHIR, similar SAG and AA and differentiation by AA, AMPc, BDNF, GDNF, ACT-A, TGFb and DAPT, e stands for embedding. (**B**) Representative image of neurite outgrowth - differentiation cloud - in condition B9000. Image shows magnified version of **S2F** (**C**) Size in µm (measured on brightfield images shown in **1G**, and **S**2F using ZeissBlue) of the differentiation cloud at 10 days of organoid production for the three conditions A, B and C. Mean ±SEM for the cell line K7, from three batches, three technical replicates and five sizes n=45. (**D**) Representative images of size measurements in organoids at the day before embedding, also represented in **S2D**. (**E**) Quantification of the colony diameter (using ZeissBlue) shown in D for K7, starting from 1000, 2000, 3000, 6000 and 9000 cells. Average diameter ±SEM for all three conditions A, B and C, from three batches and three technical replicates, n=27. (**F**) Same as **E** grouped by condition A, B and C. Average diameter ±SEM for all five input cell numbers, from three batches and three technical replicates, n=45. (**G**) Representative images of organoids 2 days after embedding. (**H** and **I**) Same as **E** and **F** only 2 days after embedding also represented in **S2G**. (**J**) Representative images of 30-day-old, free floating organoids from K7 stained for TH 488, and Hoechst 405 also represented in **S2K**. (**K**) Quantification of the area of Hoechst from **J** for all five input cell numbers and all three conditions. Mean ±SEM of three batches n=3. (**L**) Quantification of the area of Hoechst in **J** grouped by conditions A, B and C. Mean ±SEM of all five input cell numbers from three batches n=15. (**A-L**) Statistical significance of Turkey's multiple comparisons *p<0.05, **p<0.01 and ***p<0.001 after one-way ANOVA.

Figure 2. Organoid density is reduced in condition B.

(**A**) Maximal intensity projections of 205 µm Z-stacks taken at the edge of the organoid with the 5x objective in a TH 488 whole mount stain and its 3D reconstruction (Imaris). Organoids were generated

from K7, starting from 1000, 2000, 3000, 6000 and 9000 cells for all three conditions A, B and C in three batches. (**B and C**) Density was calculated from **A** by Volume TH/Volume cylinder (area of organoid and height of stack) for all five input cell numbers and all three conditions **B** or grouped by condition **C**. (**B**) Mean ±SEM of three batches n=3. (**C**) Mean ±SEM of all five input cell numbers in three batches n=15. (**D**) Horizontal plan of whole mount TH 488 stained organoids taken with a 5x objective. Organoids were generated from K7, starting from five input cell numbers for all three conditions A, B, and C in three batches. Antibody penetration was measured using the height of the fluorescent signal for all cell numbers and all three conditions **E** and grouped by conditions **F**. (**E**) Mean ±SEM for three batches n=3. (**F**) Mean ±SEM for five input cell numbers and three batches n=15.

(**G – I**) TH network quantification for all three conditions A, B and C in all three cell lines K7, T12 and COR at day 30 of differentiation. Volume Hoechst and Volume TH were quantified in wholemount stainings using Imaris software as show in Figure 5A. (**G**) Graphical representation of reduced density in B compared to A. (**H**) Non-normalized volumes of whole mount stains for TH show no differences between conditions, n=3 cell lines. One-way ANOVA. (**I**) Number of Hoechst positive cells is reduced in condition B, n=3 cell lines. One-way ANOVA p≤0.01 **. Meaning that condition B has a reduced density compared to A as summarized in (**G**).

(**A-I**) Statistical significance of Turkey's multiple comparisons *p<0.05, **p<0.01 and ***p<0.001 after one-way ANOVA.

Figure 3. Further protocol optimization enables whole mount stainings in all three conditions

Representative whole mount stained organoids for conditions A6000, B9000 and C3000 at day 30 of differentiation after 8 min acetone step was added. Stainings were done using TH 488, TUJ1 647, FOXA2 568, and Hoechst 405 for all three cell lines K7, T12, COR.

Figure 4. Cell death is reduced in condition B

(**A**) Bright field images of the cellular bodies of organoid sections from K7, starting from 1000, 2000, 3000, 6000 and 9000 cells for all three conditions A, B and C. (**B**) The quantification of the dead core area showing no dead core in B and below C3000. (**C** and **D**) The area of the dead core is further quantified for all three cell lines K7, T12 and COR for the conditions A6000, B9000, and C3000 and three batches. Mean ±SEM n=9 either grouped by condition **C** or cell line **D**. (**E**) The dead core was also quantified in the whole mount stains of (**Figure 3**). (**F** and **G**) Pyknotic nucleis were counted in whole mount stainings using Imaris for A6000, B9000, and C3000 and for three cell lines K7, T12 and COR and three batches. Pyknotic nucleis were normalized to total cell count. Mean ±SEM n=9 either grouped by condition **F** or cell line **G**. (**H**) Live cells were counted in whole mount stainings using Imaris for A6000, B9000, and C3000 and for three cell lines K7, T12 and COR and three batches. (**I** and **J**) ATP luminescence was normalized to the diameter of the organoid for A6000, B9000, and C3000 and for three different cell lines K7, T12 and COR and three batches. The graphs show the mean ±SEM n=9 either grouped by condition **I** or cell line **J**. (**A-J**) Statistical significance of Turkey's multiple comparisons *p<0.05, **p<0.01 and ***p<0.001 after one-way ANOVA.

Figure 5. The proportion of differentiated cells is increased in condition B compared to A

(**A-N**) Quantification and representation of immunostained Zeiss confocal images in whole mount stains **A** or sections **B** of 30 day old organoids for all three conditions A6000, B9000 and C3000 and for and all three cell lines K7, T12 and COR. (**A**) 3D reconstruction of whole mount staining for neuronal marker TUJ1 647 and TH 488, and midbrain marker FOXA2 568 using Imaris software. (**B**) Reconstructed masks of sections stained for TUJ1, GFAP, S100ß, SOX2, and Ki67 using Matlab. (**C**) Graphical representation of the shape of the organoid and the different plans. (**D, E, F, J**) Quantification of whole mounts stains. Mean ±SEM n=3 for each quantification either grouped by condition **D, F** and **J** or cell line **E**. (**GI, H, I, K, L**) Quantification of sections for three independent

24

batches grouped by condition, mean ±SEM n=9. (**GII**) Percentage resulting from **GI** applied on alive cell

count from **Fig. 3H** (**D-L**) Statistical significance of Turkey's multiple comparisons *p<0.05, **p<0.01

and ***p<0.001 after one-way ANOVA, except **F** significance p<0.05 in one-way ANOVA but not in

multiple comparisons. (**M-O**) Representative image of staining quantified in **A** and **B**. Staining's for TH

488, Map2 647, FOXA2 568, GFAP 647, S100ß 568, SOX2 647, and Ki67 488. (**P** and **Q**) Variability

analysis. The coefficient of variation is significantly reduced in condition B compared to A when

comparing three cell lines, three batches, and 9 experimental data sets. Average CV ±SEM across cell

lines **A** or batches **B**, n=27. Statistical significance *p<0.05, **p<0.01 and ***p<0.001 paired t-test.

Figure 6. Condition B shows different cellular identities and midbrain functionality

(**A-F**) Immunostainings in whole mount organoids of K7, T12 and COR from condition B9000. (**A** and

B) Expression of vesicular glutamate transporter 2 (GLUT) 568 **A** and serotonin (SERO) 568 **B** is shown

together and independent of TH 488. (**C, D** and **E**) Organoids co-express TH 488 with GIRK 647 **C**,

dopamine transporter DAT 568 **D** or Dopamine (DOPA) 488 **E**. (**F**) Postsynaptic protein 95 488 and

synaptophysin 568 are expressed within the neurites of the TH positive 647 neuronal network.

Figure 7. The optimized organoid model recapitulates toxin-induced neurodegeneration.

(**A - E**) Organoids for condition B9000 were treated with 50, 100, 150 and 175 µM 6-OHDa at day 30

of differentiation. (**A**) No difference in glial cell abundance (GFAP 568) normalized to nuclear volume

(Hoechst 405). (**B**) Representative images of neurodegeneration at 175 µM. (**C**) Decrease in

dopaminergic neurons (TH 488) from 100 µM 6-OHDa on, compared to control. (**D**) No significant

decrease in total neurons (TUJ1 647) compared to control. (**E**) Specific decrease in dopaminergic

neurons compared to total amount of neurons. (**A, C-E**) The graphs show the mean ±SEM of the three

cell lines K7, T12, COR n=3. Statistical significance of Turkey's multiple comparisons *p<0.05, **p<0.01
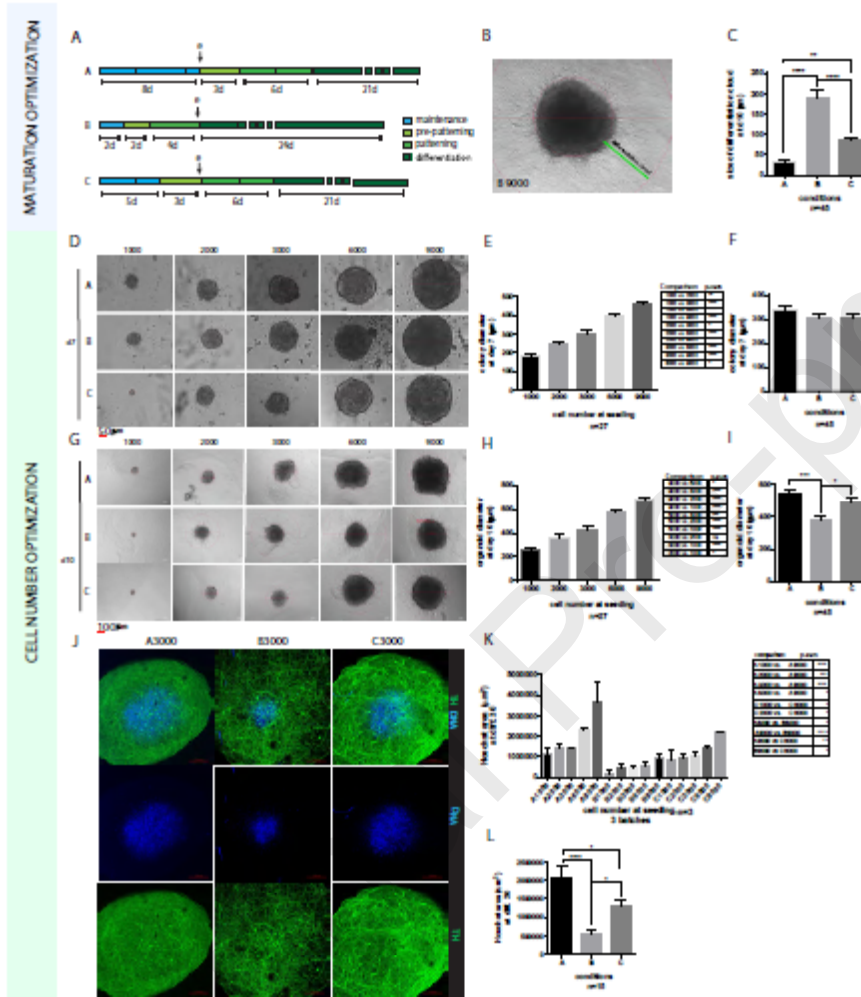
and ***p<0.001 after one-way ANOVA.

Figure 1.

ANTIBODY PENETRATION
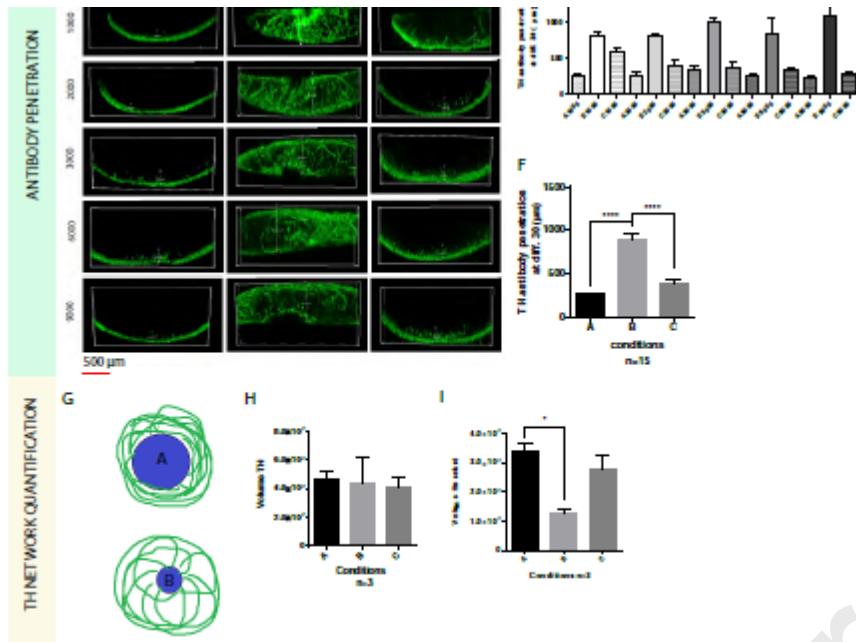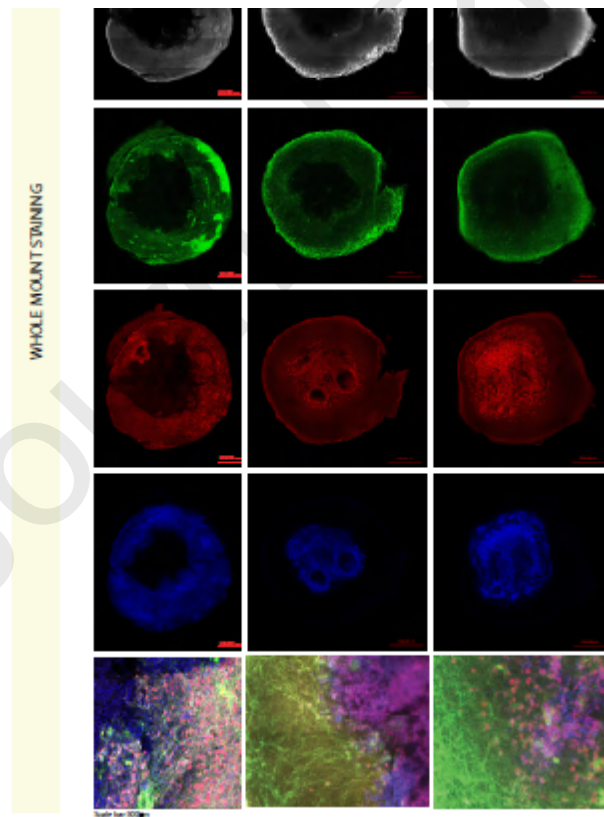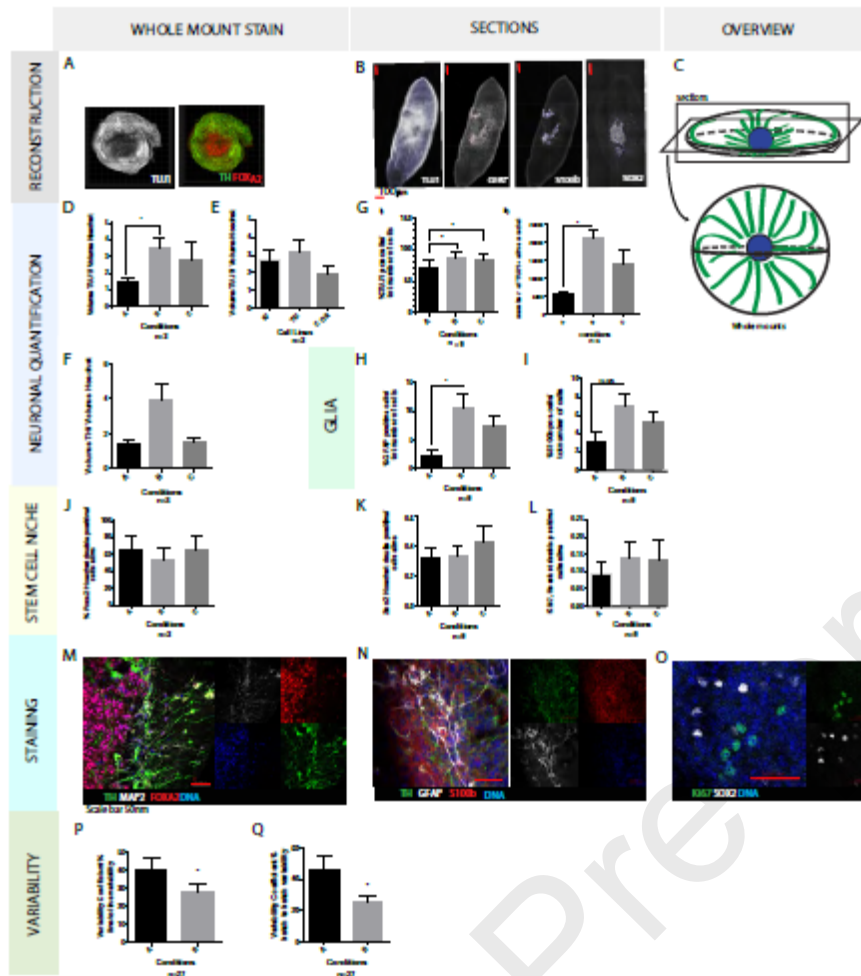
TH NETWORK QUANTIFICATION

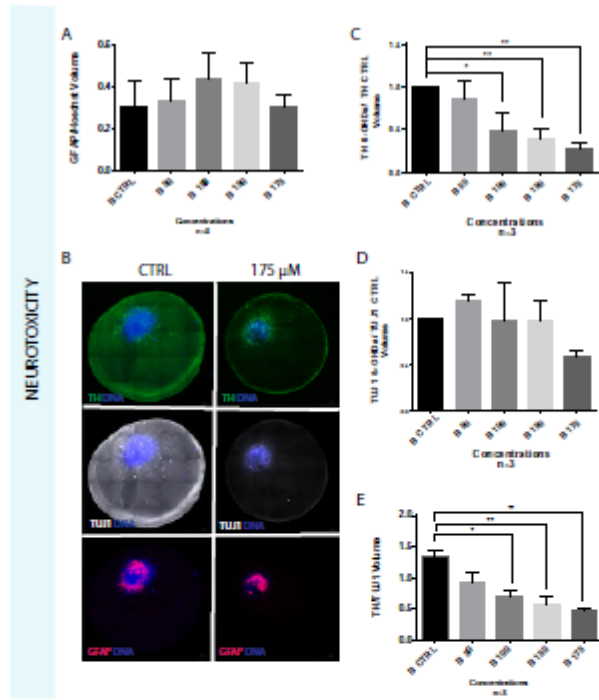Figure 2.

WHOLE MOUNT STAINING

Figure 3

Figure 4.

Figure 5.

Figure 6.

Figure 7.